

This discussion paper is/has been under review for the journal Atmospheric Chemistry and Physics (ACP). Please refer to the corresponding final paper in ACP if available.

Optical and microphysical characterization of aerosol layers over South Africa by means of multi-wavelength depolarization and Raman lidar measurements

E. Giannakaki^{1,a}, P. G. van Zyl², D. Müller³, D. Balis⁴, and M. Komppula¹

¹Finnish Meteorological Institute, P.O. Box 1627, 70211, Kuopio, Finland

²Unit for Environmental Sciences and Management, North-West University,
Potchefstroom, South Africa

³School of Physics, Astronomy and Mathematics, University of Hertfordshire, Hatfield, UK

⁴Laboratory of Atmospheric Physics, Thessaloniki, Greece

^aon leave from: Department of Environmental Physics and Meteorology, Faculty of Physics,
University of Athens, Athens, Greece

ACPD
15, 35237–35276, 2015

Optical and
microphysical
characterization of
aerosol layers

E. Giannakaki et al.

Title Page	
Abstract	Introduction
Conclusions	References
Tables	Figures
◀	▶
◀	▶
Back	Close
Full Screen / Esc	
Printer-friendly Version	
Interactive Discussion	



Received: 16 November 2015 – Accepted: 23 November 2015

– Published: 15 December 2015

Correspondence to: E. Giannakaki (eleni.giannakaki@fmi.fi)

Published by Copernicus Publications on behalf of the European Geosciences Union.

ACPD

15, 35237–35276, 2015

Optical and
microphysical
characterization of
aerosol layers

E. Giannakaki et al.

Title Page

Abstract

Introduction

Conclusions

References

Tables

Figures



Back

Close

Full Screen / Esc

Printer-friendly Version

Interactive Discussion

Abstract

Optical and microphysical properties of different aerosol types over South Africa measured with a multi-wavelength polarization Raman lidar are presented. This study could assist in bridging existing gaps relating to aerosol properties over South Africa, since limited long-term data of this type is available for this region. The observations were performed under the framework of the EUCAARI campaign in Elandsfontein. The multi-wavelength Polly^{XT} Raman lidar system was used to determine vertical profiles of the aerosol optical properties, i.e. extinction and backscatter coefficients, Ångström exponents, lidar ratio and depolarization ratio. The mean microphysical aerosol properties, i.e. effective radius and single scattering albedo were retrieved with an advanced inversion algorithm. Clear differences were observed for the intensive optical properties of atmospheric layers of biomass burning and urban/industrial aerosols. Our results reveal a wide range of optical and microphysical parameters for biomass burning aerosols. This indicates probable mixing of biomass burning aerosols with desert dust particles, as well as the possible continuous influence of urban/industrial aerosol load in the region. The lidar ratio at 355 nm, the linear particle depolarization ratio at 355 nm and the extinction-related Ångström exponent from 355 to 532 nm were 52 ± 7 sr; 0.9 ± 0.4 % and 2.3 ± 0.5 , respectively for urban/industrial aerosols, while these values were 92 ± 10 sr; 3.2 ± 1.3 %; 2.0 ± 0.4 respectively for biomass burning aerosols layers. Biomass burning particles are larger and slightly less absorbing compared to urban/industrial aerosols. The particle effective radius were found to be 0.10 ± 0.03 , 0.17 ± 0.04 and 0.13 ± 0.03 μm for urban/industrial, biomass burning, and mixed biomass burning and desert dust aerosols, respectively, while the single scattering albedo at 532 nm were 0.87 ± 0.06 , 0.90 ± 0.06 , and 0.88 ± 0.07 (at 532 nm), respectively for these three types of aerosols. Our results were within the same range of previously reported values.

Optical and microphysical characterization of aerosol layers

E. Giannakaki et al.

[Title Page](#)

[Abstract](#)

[Introduction](#)

[Conclusions](#)

[References](#)

[Tables](#)

[Figures](#)

◀

▶

[Back](#)

[Close](#)

[Full Screen / Esc](#)

[Printer-friendly Version](#)

[Interactive Discussion](#)



1 Introduction

Atmospheric aerosols of natural and anthropogenic origin contribute substantially to global climate variability (IPCC, 2013). Currently, the magnitude of the (anthropogenic) aerosol impact on climate causes the largest uncertainty on our knowledge of climate change (Forster et al., 2007). Large uncertainties exist due to the diversity, not only with respect to aerosol particle size, composition, sources and lifetime variation, but also with regard to the spatial and temporal distributions of aerosols. Thus, the impacts of aerosols on climate must be understood and quantified on a regional scale rather than on a global-average basis (Piketh et al., 2002).

High-quality aerosol measurements in the Southern Hemisphere are rather limited. South Africa is located at the southernmost tip of the African continent, extending from 22 to 34° S latitude and from 16 to 32° E longitude. Previous studies have indicated that South Africa is one of the countries in the world that is largely affected by aerosol load, due to various natural and anthropogenic sources (Piketh et al., 2000, 2002; Formenti et al., 2002, 2003; Campbell et al., 2003; Eck et al., 2003; Freiman and Piketh, 2003; Ichoku et al., 2003; Ross et al., 2003; Winkler et al., 2008; Queface et al., 2011; Tesfaye et al., 2011; Venter et al., 2012; Tiitta et al., 2014). Intensive efforts have been undertaken during recent years to characterize aerosol pollution in South Africa. In general, previous studies pointed at the importance of regional circulation of air masses and seasonal pollutant variation. The optical properties of aerosols have been studied by means of sun photometers (e.g. Queface et al., 2011; Eck et al., 2003), in situ data (e.g. Laakso et al., 2012) and satellite observations (e.g. Tesfaye et al., 2011) in these studies, which are based on columnar aerosol optical properties. Ground-based Raman lidars provide vertically resolved information on the distribution and optical properties of aerosols. Giannakaki et al. (2015) used Raman lidar data obtained over a one year period at Elandsfontein in South Africa (26°15' S, 29°26' E, 1745 m a.s.l.) to study the geometrical characteristics, intensive and extensive optical properties of free-tropospheric aerosol layers. In addition to these characteristics that

Optical and microphysical characterization of aerosol layers

E. Giannakaki et al.

[Title Page](#)

[Abstract](#)

[Introduction](#)

[Conclusions](#)

[References](#)

[Tables](#)

[Figures](#)



[Back](#)

[Close](#)

[Full Screen / Esc](#)

[Printer-friendly Version](#)

[Interactive Discussion](#)



can be determined with lidar data, multi-wavelength Raman lidar measurements can also be used to determine profiles of microphysical particle properties by using inversion algorithms (Twomey, 1977; Veselovskii et al., 2002; Müller et al., 2001). In this study we expand our study of aerosols in South Africa by providing information on the 5 microphysical and optical properties of aerosol layers. This type of aerosol lidar observations are valuable for spaceborne lidars such as CALIPSO (Cloud–Aerosol Lidar and Infrared Pathfinder Satellite Observations) (e.g. Omar et al., 2009), since lidar ratio values for different aerosol types are required for reliable aerosol extinction retrievals. Therefore, this study could be useful for further improving lidar ratio selection-scheme 10 algorithms used in spaceborne lidar missions.

Four long-term ground-based aerosol measurements were carried out at sites in economically growing countries in Asia, Africa and South America within the EUCAARI project (Kulmala et al., 2011), which included Elandsfontein in South Africa. The aim of EUCAARI was to characterize particles in terms of physical, optical and chemical 15 aerosol properties. Here we report lidar observations that were performed at Elandsfontein. In particular, we discuss the optical and microphysical properties of aerosol layers that are caused by biomass burning and urban/industrial activities at the site. We present aerosol lidar ratios, particle linear depolarization ratios and Ångström exponents for biomass burning and urban/industrial aerosol layers measured with a multi-wavelength Raman lidar. The effect of desert dust particles on biomass burning aerosol 20 layers in terms of the intensive optical and microphysical properties is also studied. In addition, effective radius and single-scattering albedo are calculated with an advanced inversion algorithm.

The paper is organized as follows: in Sect. 2, the research site, the methodology 25 used for the retrieval of optical and microphysical properties and the aerosol typing are introduced. As a case study, the arrival of a biomass burning aerosol layer over Elandsfontein is discussed in Sect. 3. Section 4 presents the main findings of the optical and microphysical aerosol properties for selected biomass burning and urban/industrial aerosol layers. We close our contribution with a summary and conclusion in Sect. 5.

Optical and microphysical characterization of aerosol layers

E. Giannakaki et al.

[Title Page](#)

[Abstract](#)

[Introduction](#)

[Conclusions](#)

[References](#)

[Tables](#)

[Figures](#)

◀

▶

[Back](#)

[Close](#)

[Full Screen / Esc](#)

[Printer-friendly Version](#)

[Interactive Discussion](#)



2 Location and methodology

2.1 Measurement site

The measurement site was located on a hill top at Elandsfontein ($26^{\circ}15' S$, $29^{\circ}26' E$, 1745 m.a.s.l.) in the Highveld region of South Africa. The station was located approximately 150 km east of the Johannesburg–Pretoria megacity, which is the largest metropolitan area in South Africa with a population of more than 10 million people (Lourens et al., 2012).

In South Africa, anthropogenic atmospheric emissions are predominantly the product of industrial activities and biomass burning (Ross et al., 2003). South Africa is the most industrialized country of the sub-continent – primarily due to the industrialized Highveld region (Freiman, 2003; Wenig et al., 2003). This region has clusters of industrial complexes and power plants between $25.5^{\circ} S$, $27.5^{\circ} E$ and $27.0^{\circ} S$, $30.5^{\circ} E$ (Ross et al., 2003), which contributes significantly to aerosol and trace gases pollution (Freiman et al., 2003). Tropospheric NO_2 distributions derived with SCIAMACHY (SCanning Imaging Absorption spectrOMeter for AtmosphericCHartographY) from August 2002 to March 2012 (Schneider et al., 2015) are presented in Fig. 1. The tropospheric NO_2 column density of the Highveld region in South Africa is comparable to that observed over central and northern Europe, eastern North America and Southeast Asia (Lourens et al., 2012).

In addition, emissions from biomass burning (wild fires) contribute significantly to regional emission loads (e.g. Giannakaki et al., 2015). Both, natural phenomena (lightning) and human induced activities are responsible for biomass burning (Edwards et al., 2006). The number of hotspots, with confidence levels between 80–100 %, (<http://earthdata.nasa.gov/data/nrt-data/firms/active-fire-data>), in the latitude range between -40 and 40° and longitude range between -20 and 60° are plotted in Fig. 2. The number of hotspots is averaged in terms of 3 months for the year 2010. Wild fires originate in the sub-equatorial central African region and progress south-

Title Page	
Abstract	Introduction
Conclusions	References
Tables	Figures
	
	
Back	Close
Full Screen / Esc	
Printer-friendly Version	
Interactive Discussion	



ward (Roy et al., 2005). In southern Africa, the fires progress along a north-west to south-east track.

2.2 Description of the lidar system and lidar data processing

The transportable aerosol Raman lidar Polly^{XT} that was operated remotely at Elandsfontain is described by Althausen et al. (2009) and Engelmann et al. (2015). Polly^{XT} works with a Nd:YAG laser emitting at its primary wavelength of 1064 nm, which after frequency doubling and tripling emits at the wavelengths of 532 and 355 nm, respectively. The receiver consists of a Newtonian telescope with a diameter of 300 mm and a field of view of 1 mrad. Photomultiplier tubes (PMT) are used for the detection of the elastically backscattered photons at 355, 532 and 1064 nm, as well as the in-elastically backscattered photons at 387 and 607 nm that correspond to the Raman-shift by nitrogen molecules at 355 and 532 nm, respectively. Additionally, the cross-polarized component at 355 nm is detected and consequently allows for the determination of the linear particle depolarization ratio (also called depolarization ratio). The vertical resolution of the signal profiles is 30 m and the raw data are typically stored as 30 s average values (20 Hz laser frequency). Data were collected on the web page of PollyNet (<http://polly.tropos.de>) where the “quicklooks” of all measurements are available.

Extinction and backscatter coefficient profiles at 355 and 532 nm, respectively, were obtained with the Raman method (Ansmann et al., 1992), while the backscatter coefficient at 1064 nm was determined by using the Klett method (Klett, 1981). An overlap correction was applied on the basis of a simple technique proposed by Wandinger and Ansmann (2002). The depolarization ratio, i.e. the ratio of the cross-polarized to the parallel-polarized component of the backscatter coefficient (particles and molecules) at 355 nm was also calculated. The contribution of the molecules can easily be calculated, which then provides the linear particle depolarization ratio (Cairo et al., 1999; Murayama et al., 1999). The overall relative errors of the lidar-derived aerosol properties range between 5–15 % for the backscatter coefficients, 10–30 % for the extinction

Title Page

Abstract

Introduction

Conclusions

References

Tables

Figures

◀

▶

Back

Close

Full Screen / Esc

Printer-friendly Version

Interactive Discussion



coefficients, 15–40 % for the lidar ratios and approximately 5–10 % for the linear particle depolarization ratio (Hänel et al., 2012).

The layer identification was based on the assumption that the optical properties should be relatively stable. This means that within a chosen height layer, the variability of the optical data should be less than the statistical uncertainty of the individual data points. In Table 1 we provide information regarding the elevated layers that were selected for the optical and microphysical aerosol characterization. The characterization of aerosol types will be discussed in Sect. 2.4.

2.3 Retrieval of microphysical properties

- Microphysical particle properties are derived with an inversion algorithm that has been developed at the Leibniz Institute for Tropospheric Research. A detailed description of the inversion code is given by Müller et al. (1999a, b). A minimum of three backscatter coefficients (355, 532, and 1064 nm) and two extinction coefficients (355 and 532 nm), with measurement errors less than 20 %, are required as input in order to obtain microphysical results that have reasonably low uncertainties (Müller et al., 2001). The selection of the individual inversion solutions is based on the concept that the back-calculated optical data should agree with the original data within the limits of the measurement errors, and that a pre-selected discrepancy level, which is an output parameter of the inversion algorithm (Müller et al., 1999a), is not exceeded. The mean particle size in terms of the effective radius is then calculated along with the standard deviation from these selected individual solutions. One also obtains a range of complex refractive indexes by applying this method. The complex refractive index is a wavelength-independent quantity. Therefore, inversion can only provide a wavelength-independent value that represents the entire range of wavelengths from 355–1064 nm. The single-scattering albedo can then be calculated from the volume concentration distribution, which is another data product of the inversion algorithm, and the associated mean complex refractive index by means of a Mie scattering algorithm.

Title Page	
Abstract	Introduction
Conclusions	References
Tables	Figures
	
	
Back	Close
Full Screen / Esc	
Printer-friendly Version	
Interactive Discussion	



Title Page

Abstract

Introduction

Conclusions

References

Tables

Figures

◀

▶

◀

▶

Back

Close

Full Screen / Esc

Printer-friendly Version

Interactive Discussion



Uncertainties associated with the retrievals are in general < 30 % for effective radius. The real part of the complex refractive index is derived to an accuracy better than ±0.1, while the imaginary part is obtained for its correct order of magnitude if the value is < 0.01*i* (for larger values of the imaginary part the uncertainty is < 50 %). The single-scattering albedo can be calculated with an accuracy of ±0.05, if uncertainties of the input optical data are on average < 10–15 %. A detailed error analysis is presented by Müller et al. (1999b, 2001) and Veselovskii et al. (2002, 2004).

2.4 Aerosol classification

The identification of the source of aerosol particles is possible with the synergetic use of in-situ and satellite measurements, as well as utilising model estimations.

The HYSPLIT_4 (Hybrid Single Particle Langrangian Integrated Trajectory) model (Draxler and Hess, 1997) was used to compute backward air mass trajectories employing the kinematic approach and by using the re-analysed National Oceanic and Atmospheric Administration (NOAA) dataset with a resolution of 2.5° × 2.5° (latitude, longitude) as input. Four-day backward trajectories were selected, because they extend far enough back in time and distance to cover the main source regions suspected to affect the region investigated. The trajectories were calculated for the center of the layer observed and for the time of the lidar measurement (see Table 1).

The number of fire hotspots is given by Moderate Resolution Imaging Spectroradiometer (MODIS) collection-5 active-fire product data (Giglio et al., 2010). The number of hotspots, obtained from MODIS for four days prior to each of the measurements, was superimposed on the trajectory analysis map in order to detect the presence of smoke particles over our site for the cases analyzed.

Trace gases were measured as part of routine air quality monitoring at the site by the national electricity supplier, i.e. Eskom. A Thermo Electron 43C SO₂ analyser and a Thermo Electron 42i NO_x analyser were used to measure SO₂ and NO_x respectively. H₂S was measured with a Thermo Electron 43A SO₂ analyzer with a Thermo Electron 340 converter. 15 min data were averaged for the extent of measurement time

for each of the measurements periods (Table 1). For instances where the combined use of trajectory analysis and fire hotspots did not indicate the presence of biomass burning aerosols we checked whether the measured NO_x , SO_2 or H_2S concentrations were higher than the seasonal mean values of that measured for the entire period of the EUCAARI campaign. These seasonal mean values are presented in Laakso et al. (2012). In addition, when the trace gases concentrations were lower than the mean seasonal values measured during the EUCAARI campaign and biomass-burning activity or desert dust advection were absent, we checked if the daily concentration of the trace gases exceeded the mean critical values.

There were also cases that indicated desert dust aerosol particles in addition to the smoke, which originated either from the Kalahari or the Namibia desert that could have additionally contributed to the aerosol loads. Therefore, the measured aerosol optical properties determined for these cases were attributed to a mixed state of biomass burning and desert dust aerosols.

An example of a measurement of biomass burning aerosols is discussed in the subsequent section in order to demonstrate the methodology used to derive the optical and microphysical aerosol properties.

3 Biomass burning aerosols on 1 October 2010 at Elandsfontein, South Africa

In Fig. 3, the time-height plot of the range-corrected signal at 1064 nm is presented for the 1 October 2010. The figure reveals a geometrically deep layer that extends up to 2.1 km height a.g.l.. The atmospheric structure, in terms of range corrected signals, is quite stable which indicates similar optical properties throughout the layer. High backscatter returns are observed on the day when the measurement is conducted in relation to the previous and the next day.

In Fig. 4, four-day backward trajectories arriving at Elandsfontein at 00:00, 02:00 and 04:00 UTC are presented. The trajectories are computed for arrival heights of 1000 and 1500 m (a.g.l.). The MODIS fire hotspots product is superimposed on the trajectory

Optical and microphysical characterization of aerosol layers

E. Giannakaki et al.

[Title Page](#)

[Abstract](#)

[Introduction](#)

[Conclusions](#)

[References](#)

[Tables](#)

[Figures](#)

◀

▶

[Back](#)

[Close](#)

[Full Screen / Esc](#)

[Printer-friendly Version](#)

[Interactive Discussion](#)



plot for the four day period. Several fires were active during the period 28 September 2010–1 October 2010 as shown in Fig. 4. The trajectory analysis for the day of the measurement reveals that the air masses were either coming from northeasterly or from northwesterly directions. It is therefore highly possible that these air masses carried smoke particles to Elandsfontein.

In Fig. 5 the optical lidar profiles are presented. The backscatter and extinction maximum at all three wavelengths was observed within the 0.9 to 1.9 km height range. High values of the lidar ratio of 96 ± 5 sr at 355 nm and 89 ± 5 sr at 532 nm indicate that the smoke particles inside this layer were most likely highly light-absorbing. The Ångström exponent, related to extinction between 355 and 532 nm, was 1.8 ± 0.1 , which points to comparably small particles and indicative of fresh smoke. A constant particle depolarization ratio in the order of 4 % is observed at 355 nm throughout the layer. The lack of significant vertical variability of the lidar ratio, the Ångström exponent and the particle depolarization ratio suggests the presence of the same type (biomass burning) of aerosols throughout the layer.

The mean values of extinction (at 355 and 532 nm) and backscatter coefficients (at 355, 532 and 1064 nm) were calculated within the defined layer and were used as input in the inversion algorithm. Effective radius, complex refractive index and single-scattering albedo were calculated with the microphysical inversion code. An effective radius of $0.15 \pm 0.02 \mu\text{m}$ was determined, while the single-scattering albedo was approximately 0.86 at 532 nm that indicates relatively strong-absorbing aerosols.

4 Results and discussion

We performed optical lidar data analysis, microphysical retrievals and aerosol typing for each of the thirty eight aerosol layers listed in Table 1 in the same way as presented in the example in Sect. 3. Each aerosol layer in Table 1 was classified into one of the three aerosol types, i.e. urban/industrial, biomass burning, and biomass burning mixed with desert dust after thorough visual inspection of the backward trajectories, MODIS

Optical and microphysical characterization of aerosol layers

E. Giannakaki et al.

[Title Page](#)

[Abstract](#)

[Introduction](#)

[Conclusions](#)

[References](#)

[Tables](#)

[Figures](#)

◀

▶

◀

▶

[Back](#)

[Close](#)

[Full Screen / Esc](#)

[Printer-friendly Version](#)

[Interactive Discussion](#)



Optical and microphysical characterization of aerosol layers

E. Giannakaki et al.

[Title Page](#)

[Abstract](#)

[Introduction](#)

[Conclusions](#)

[References](#)

[Tables](#)

[Figures](#)

◀

▶

◀

▶

[Back](#)

[Close](#)

[Full Screen / Esc](#)

[Printer-friendly Version](#)

[Interactive Discussion](#)



It is evident from Fig. 6 that Ångström exponent values for the different aerosol types overlap. Therefore, another intensive aerosol property, the linear particle depolarization ratio, which is an indicator of non-spherical particles, was also used. Figure 7 shows the lidar ratio at 355 nm vs. the depolarization ratio at the same wavelength for the three aerosol types. Different clusters of data pairs can be identified. Lower depolarization ratio values were found for urban/industrial aerosol layers. These aerosol layers are also characterized by lower lidar ratios and thus the data points representing anthropogenic pollution occupy the lower left region in Fig. 6. Significantly larger particle linear depolarization ratios with a mean of $8.3 \pm 0.7\%$ were found for mixed biomass burning and desert dust aerosols. Typical desert dust aerosol depolarization ratios determined in field measurements performed in the northwestern corner of the Sahara ranged from 30 to 35 % at 532 nm with a mean value of $31 \pm 3\%$ (Freudenthaler et al., 2009). In addition, particle depolarization ratios ranging between 30 to 35 % were also observed for Asian desert dust (Sugimoto et al., 2003; Shimizu et al., 2004; Shin et al., 2015) and desert dust originating from Middle East dust sources (Mamouri et al., 2013). Depolarization ratios of the mixtures of biomass burning aerosols and desert dust particles determined for African biomass burning and dust mixtures ranged between 8–26 % at 532 nm (Weinzierl et al., 2011; Tesche et al., 2009). Therefore depolarization values reported in this study are at the lower end of these values. This observed difference can be attributed to the different contribution of desert dust particles to the biomass burning plume. However, we should also note that the geometrical shape of the dust particles over the Kalahari desert could be different from the shape of Saharan dust.

A wide range of (lower) depolarization ratios and lidar ratios was found for biomass burning aerosols. This observed variability can be attributed to differences in the chemical composition of the particles that depends on the source region, relative humidity in the atmosphere, the type of fire, or the combined effect of these factors. In addition, the mixing of the biomass burning aerosols with maritime or even urban/industrial background aerosols cannot be excluded as a possible reason for the variability of lidar ratio and depolarization ratio values.

Optical and microphysical characterization of aerosol layers

E. Giannakaki et al.

[Title Page](#)

[Abstract](#)

[Introduction](#)

[Conclusions](#)

[References](#)

[Tables](#)

[Figures](#)

◀

▶

◀

▶

[Back](#)

[Close](#)

[Full Screen / Esc](#)

[Printer-friendly Version](#)

[Interactive Discussion](#)



Several statistics of lidar ratios and Ångström exponents for different aerosol types in the world are available for comparison. Figure 8 provides some of the general literature with regard to the lidar ratios values at 355 nm and Ångström exponents of urban/industrial and biomass-burning aerosols, as well as for mixtures of biomass burning and desert dust aerosols. It is evident from Fig. 8 that intensive aerosol properties are in good agreement with values found from other studies.

The lidar ratio at 355 nm, in particular, shows similar values for anthropogenic aerosols in various regions of the world. Ångström exponent values found for urban/industrial particles in this study are at the upper limit of results previously published for this aerosol type, which indicates slightly smaller particles at Elandsfontein that can most probably be ascribed by differences in the emission sources. The depolarization ratio is at the lower limit indicating spherically shaped anthropogenic particles.

The lidar ratio for biomass burning aerosol layers is within the range of previously reported values, although the values tend to be more at the upper limit of the reported values. The Ångström exponents are in very good agreement with previous studies. Müller et al. (2007) studied the growth of free-tropospheric forest fire smoke particles and indicated that the Ångström exponent decreases with the duration of transport. The Ångström exponent values found in this study (1.7 ± 0.3) corresponds to travel times of the biomass burning aerosols between 1 and 3 days, which is confirmed by back-ward trajectory analysis. The characteristics of biomass burning emissions in the subtropical South African region vary according to the type of fuel burned (vegetation type), meteorology and combustion phase (Ross et al., 2003). For example, flaming grass fires produce smoke with more soot compared to smoke emitted from smoldering wood and bush fires (Posfai et al., 2003). Thus differences in the chemical composition of the particles might be one of the reasons for the observed large lidar ratio.

For the biomass burning mixed with desert dust type aerosols the lidar ratio values reported here are in very good agreement with previous studies. The contribution of desert dust particles within the observed biomass burning plumes is probably lower, thus resulting in a lower depolarization ratio and larger Ångström exponent than what

Optical and microphysical characterization of aerosol layers

E. Giannakaki et al.

[Title Page](#)

[Abstract](#)

[Introduction](#)

[Conclusions](#)

[References](#)

[Tables](#)

[Figures](#)

◀

▶

◀
Back

▶
Close

[Full Screen / Esc](#)

[Printer-friendly Version](#)

[Interactive Discussion](#)



has been reported in literature for biomass burning mixed with dust as mentioned previously. Groß et al. (2011) reported neutral wavelength-dependence of the particle depolarization ratios for mixed dust and smoke layers for which Ångström exponents varied between 0.12 and 0.16, while Tesche et al. (2011) reported wavelength-independent linear particle depolarization ratios of 0.12–0.18 at 355, 532 and 710 nm for mixed dust and smoke layers. In that sense our results on particle depolarization ratios at 355 nm are similar to results from these studies reporting linear particle depolarization ratio at 532 nm.

In Fig. 9 the effective radius against the Ångström exponent is plotted. In general the plot shows the same features already noted for Fig. 6. On average the largest aerosols are determined for biomass burning aerosols (red) with an effective radius of $0.17 \pm 0.04 \mu\text{m}$. Particles from anthropogenic pollution (black) are smaller with a mean effective radius of $0.1 \pm 0.03 \mu\text{m}$. Our results indicate that the influence of Kalahari desert dust on biomass burning plumes leads to smaller particles compared to pure biomass burning aerosols with a mean effective radius of $0.13 \pm 0.03 \mu\text{m}$.

Mean microphysical properties i.e. effective radius, single scattering albedo and complex refractive index are listed with their associated standard deviations, ranges (minimum and maximum values) and medians in Table 3. The particles in the biomass-burning aerosol layers show a mean effective radius of $0.17 \pm 0.04 \mu\text{m}$, which is within the range of values reported in previous studies for biomass burning aerosols. Reid et al. (1998) reported count median diameter values ranging from $0.12 \mu\text{m}$ for fresh particles to $0.21 \mu\text{m}$ for aged particles near rain-forest fires in Brazil. Radke et al. (1988) obtain values of approximately $0.22 \mu\text{m}$ for particles from forest fires in North America. Wandinger et al. (2002) found larger biomass burning aerosols with an effective radius of approximately $0.25 \mu\text{m}$. Effective radii in the range between 0.19 and $0.44 \mu\text{m}$ were found for biomass burning aerosol layers resulting from long-range transport across Romania (Nicolae et al., 2013). Müller et al. (2007) presented values ranging between 0.13 and $0.15 \mu\text{m}$ for plumes ageing between one to three days.

Optical and microphysical characterization of aerosol layers

E. Giannakaki et al.

[Title Page](#)

[Abstract](#)

[Introduction](#)

[Conclusions](#)

[References](#)

[Tables](#)

[Figures](#)

◀

▶

[Back](#)

[Close](#)

[Full Screen / Esc](#)

[Printer-friendly Version](#)

[Interactive Discussion](#)



Optical and microphysical characterization of aerosol layers

E. Giannakaki et al.

[Title Page](#)

[Abstract](#)

[Introduction](#)

[Conclusions](#)

[References](#)

[Tables](#)

[Figures](#)

◀

▶

◀

▶

[Back](#)

[Close](#)

[Full Screen / Esc](#)

[Printer-friendly Version](#)

[Interactive Discussion](#)



5 Summary and conclusions

Thirty eight aerosol layers of urban/industrial, biomass burning, and mixed biomass burning and desert dust aerosols were studied with regard to their optical and microphysical properties at Elandsfontein, South Africa. The combination of Raman lidar observations with backward trajectory analysis, satellite fire observations and in situ data allowed for source identification of the elevated aerosol layers. Measurements of the lidar ratios and depolarization ratios are presented in order to assist in the separation of anthropogenic, biomass burning, and mixtures of biomass burning with desert dust particles.

A wide range of optical (lidar ratio and depolarization ratio) and microphysical (single scattering albedo, complex refractive index) properties was determined for biomass burning aerosols, indicating differences in chemical composition. Aerosols from urban and industrial activities are on average characterized by larger Ångström exponents than (pure or mixed) biomass burning aerosols. Lidar ratios for biomass burning aerosols are among the highest found in literature with a mean value of 92 ± 10 sr, while the anthropogenic aerosols are characterized by lower lidar ratios in the range between 41 and 59 sr at 355 nm. Ångström exponents were found to be similar for all types of aerosol types under study, with slightly larger values determined for anthropogenic aerosols. Mean effective radii of 0.17 ± 0.04 and 0.1 ± 0.03 μm were calculated for biomass burning and anthropogenic aerosols, respectively. We have also shown that in certain instances biomass burning aerosols may contain a small amount of desert dust particles resulting in higher depolarization ratios and lower lidar ratios than the values reported for pure biomass burning aerosols. Moderately absorbing particles were found for biomass burning layers with a mean single scattering albedo of 0.9 ± 0.06 . Biomass burning aerosols mixed with desert dust particles, were more absorbing with a mean single-scattering albedo of 0.88 ± 0.07 . A slightly lower mean single-scattering albedo of 0.87 ± 0.06 was found for urban/industrial aerosol layers. However, this value was larger than the values reported for the same site from ground-

[Title Page](#)[Abstract](#)[Introduction](#)[Conclusions](#)[References](#)[Tables](#)[Figures](#)[◀](#)[▶](#)[Back](#)[Close](#)[Full Screen / Esc](#)[Printer-friendly Version](#)[Interactive Discussion](#)

Optical and microphysical characterization of aerosol layers

E. Giannakaki et al.

[Title Page](#)

[Abstract](#)

[Introduction](#)

[Conclusions](#)

[References](#)

[Tables](#)

[Figures](#)

◀

▶

[Back](#)

[Close](#)

[Full Screen / Esc](#)

[Printer-friendly Version](#)

[Interactive Discussion](#)



Amiridis, V., Balis, D. S., Giannakaki, E., Stohl, A., Kazadzis, S., Koukouli, M. E., and Zanis, P.: Optical characteristics of biomass burning aerosols over Southeastern Europe determined from UV-Raman lidar measurements, *Atmos. Chem. Phys.*, 9, 2431–2440, doi:10.5194/acp-9-2431-2009, 2009.

5 Ansmann, A., Wandinger, U., Riebesell, M., Weitkamp, C., and Michaelis, W.: Independent measurement of extinction and backscatter profiles in cirrus clouds by using a combined Raman elastic-backscatter lidar, *Appl. Optics*, 31, 7113–7131, doi:10.1364/AO.31.007113, 1992.

10 Ansmann, A., Engelmann, R., Althausen, D., Wandinger, U., Hu, M., Zhang, Y., and He, Q.: High aerosol load over the Pearl River Delta, China, observed with Raman lidar and Sun photometer, *Geophys. Res. Lett.*, 32, L13815, doi:10.1029/2005GL023094, 2005.

15 Ansmann, A., Baars, H., Tesche, M., Müller, D., Althausen, D., Engelmann, R., Pauliquevis, T., and Artaxo, P.: Dust and smoke transport from Africa to South America: lidar profiling over Cape Verde and the Amazon rainforest, *Geophys. Res. Lett.*, 36, L11802, doi:10.1029/2009GL037923, 2009.

Baars, H., Ansmann, A., Althausen, D., Engelmann, R., Artaxo, P., Pauliquevis, T., and Souza, R.: Further evidence for significant smoke transport from Africa to Amazonia, *Geophys. Res. Lett.*, 38, L20802, doi:10.1029/2011GL049200, 2011.

20 Baars, H., Ansmann, A., Althausen, D., Engelmann, R., Heese, B., Müller, D., Artaxo, P., Paixao, M., Pauliquevis, T., and Souza, R.: Aerosol profiling with lidar in Amazon Basin during the wet and dry season, *J. Geophys. Res.*, 117, D21201, doi:10.1029/2012JD018338, 2012.

25 Balis, D. S., Amiridis, V., Zerefos, C., Gerasopoulos, E., Andreae, M., Zanis, P., Kazantzidis, A., Kazadzis, S., and Papayannis, A.: Raman lidar and Sun photometric measurements of aerosol optical properties over Thessaloniki, Greece during a biomass burning episode 2003, *Atmos. Environ.*, 37, 4529–4538, doi:10.1016/S1352-2310(03)00581-8, 2003.

30 Burton, S. P., Ferrare, R. A., Hostetler, C. A., Hair, J. W., Rogers, R. R., Oblard, M. D., Butler, C. F., Cook, A. L., Harper, D. B., and Froyd, K. D.: Aerosol classification using airborne High Spectral Resolution Lidar measurements – methodology and examples, *Atmos. Meas. Tech.*, 5, 73–98, doi:10.5194/amt-5-73-2012, 2012.

Burton, S. P., Ferrare, R. A., Vaughan, M. A., Omar, A. H., Rogers, R. R., Hostetler, C. A., and Hair, J. W.: Aerosol classification from airborne HSRL and comparisons with the CALIPSO

Title Page

Abstract

Introduction

Conclusions

References

Tables

Figures

◀

▶

◀

▶

Back

Close

Full Screen / Esc

Printer-friendly Version

Interactive Discussion



vertical feature mask, *Atmos. Meas. Tech.*, 6, 1397–1412, doi:10.5194/amt-6-1397-2013, 2013.

Cairo, F., Di Donfrancesco, G., Adriani, A., Pulvirenti, L., and Fierli, F.: Comparison of various linear depolarization parameters measured by lidar, *Appl. Optics*, 38, 4425–4432, doi:10.1364/AO.38.004425, 1999.

Campbell, J. R., Welton, E. J., Spinhirne, J. D., Ji, Q., Tsay, S. C., Piketh, S. J., Barenbrug, M., and Holben, B. N.: Micropulse lidar observations of tropospheric aerosols over northeastern South Africa during the ARREX and SAFARI 2000 dry season experiments, *J. Geophys. Res.*, 108, 8497, doi:10.1029/2002jd002563, 2003.

Draxler, R. R. and Hess, G. D.: Description of the HYSPLIT 4 Modeling System, NOAA Tech Memo, ERL ARL-224, 24, NOAA, Silver Spring, MD, USA, 1997.

Eck, T. F., Holben, B. N., Ward, D. E., Mukelabai, M. M., Dubovik, O., Smirnov, A., Schafer, J. S., Hsu, N. C., Piketh, S. J., Queface, A., Le Roux, J., Swap, R. J., and Slutsker, I.: Variability of biomass burning aerosol optical characteristics in southern Africa during the SAFARI 2000 dry season campaign and a comparison of single scattering albedo estimates from radiometric measurements, *J. Geophys. Res.*, 108, 8477, doi:10.1029/2002jd002321, 2003.

Edwards, D. P., Emmons, L. K., Gille, J. C., Chu, A., Attie, Giglio, L., Wood, S. W., Haywood, J., Deeter, M. N., Massie, S. T., Ziskin, D. C., and Drummond, J. R.: Satellite-observed pollution from Southern Hemisphere biomass burning, *J. Geophys. Res.*, 111, D14312, doi:10.1029/2005JD006655, 2006.

Engelmann, R., Kanitz, T., Baars, H., Heese, B., Althausen, D., Skupin, A., Wandinger, U., Komppula, M., Stachlewska, I. S., Amiridis, V., Marinou, E., Mattis, I., Linné, H., and Ans-mann, A.: EARLINET Raman Lidar Polly^{XT}: the neXT generation, *Atmos. Meas. Tech. Discuss.*, 8, 7737–7780, doi:10.5194/amtd-8-7737-2015, 2015.

Formenti, P., Winkler, H., Fourie, P., Piketh, S., Makgopa, B., Helas, G., and Andreae, M. O.: Aerosol optical depth over a remote semi-arid region of South Africa from spectral measurements of the daytime solar extinction and the nighttime stellar extinction, *Atmos. Res.*, 62, 11–32, doi:10.1016/s0169-8095(02)00021-2, 2002.

Formenti, P., Elbert, W., Maenhaut, W., Haywood, J., Osborne, S., and Andreae, M. O.: Inorganic and carbonaceous aerosols during the Southern African Regional Science Initiative (SAFARI 2000) experiment: chemical characteristics, physical properties, and emission data for smoke from African biomass burning, *J. Geophys. Res.*, 108, 8488, doi:10.1029/2002jd002408, 2003.

Title Page

Abstract

Introduction

Conclusions

References

Tables

Figures

◀

▶

◀
Back

▶
Close

Full Screen / Esc

Printer-friendly Version

Interactive Discussion



- Forster, P., Ramaswamy, V., Artaxo, P., Berntsen, T., Betts, R., Fahey, D., Haywood, J., Lean, J., Lowe, D., Myhre, G., Nganga, J., Prinn, R., Raga, G., Schulz, M., and Dorland, R. V.: Changes in atmospheric constituents and in radiative forcing, in: Climate Change 2007: The Physical Science Basis, Contribution of Working Group I to the Fourth Assessment Report of the Intergovernmental Panel on Climate Change, Cambridge Univ. Press, Cambridge, UK and New York, NY, USA, 129–234, 2007.
- Freiman, M. T. and Piketh, S. J.: Air transport into and out of the industrial Highveld region of South Africa, *J. Appl. Meteorol.*, 42, 994–1002, doi:10.1175/1520-0450(2003)042<0994:ATIAOO>2.0.CO;2, 2003.
- Freudenthaler, V., Esselborn, M., Wiegner, M., Heese, B., Tesche, M., Ansmann, A., Müller, D., Althausen, D., Wirth, M., Fix, A., Ehret, G., Knippertz, P., Toledano, C., Gasteiger, J., Garhammer, M., and Seefeldner, M.: Depolarization ratio profiling at several wavelengths in pure Saharan dust during SAMUM 2006, *Tellus B*, 61, 165–179, doi:10.1111/j.1600-0889.2008.00396.x, 2009.
- Giannakaki, E., Balis, D. S., Amiridis, V., and Zerefos, C.: Optical properties of different aerosol types: seven years of combined Raman-elastic backscatter lidar measurements in Thessaloniki, Greece, *Atmos. Meas. Tech.*, 3, 569–578, doi:10.5194/amt-3-569-2010, 2010.
- Giannakaki, E., Pfüller, A., Korhonen, K., Mielonen, T., Laakso, L., Vakkari, V., Baars, H., Engelmann, R., Beukes, J. P., Van Zyl, P. G., Josipovic, M., Tiitta, P., Chiloane, K., Piketh, S., Lihavainen, H., Lehtinen, K. E. J., and Komppula, M.: One year of Raman lidar observations of free-tropospheric aerosol layers over South Africa, *Atmos. Chem. Phys.*, 15, 5429–5442, doi:10.5194/acp-15-5429-2015, 2015.
- Giglio, L., Randerson, J. T., van der Werf, G. R., Kasibhatla, P. S., Collatz, G. J., Morton, D. C., and DeFries, R. S.: Assessing variability and long-term trends in burned area by merging multiple satellite fire products, *Biogeosciences*, 7, 1171–1186, doi:10.5194/bg-7-1171-2010, 2010.
- Groß, S., Tesche, M., Freudenthaler, V., Toledano, C., Wiegner, M., Ansmann, A., Althausen, D., and Seefeldner, M.: Characterization of Saharan dust, marine aerosols and mixtures of biomass-burning aerosols and dust by means of multi-wavelength depolarization and Raman lidar measurements during SAMUM 2, *Tellus B*, 63, 706–724, doi:10.1111/j.1600-0889.2011.00556.x, 2011.

Optical and microphysical characterization of aerosol layers

E. Giannakaki et al.

[Title Page](#)

[Abstract](#)

[Introduction](#)

[Conclusions](#)

[References](#)

[Tables](#)

[Figures](#)

◀

▶

◀

▶

[Back](#)

[Close](#)

[Full Screen / Esc](#)

[Printer-friendly Version](#)

[Interactive Discussion](#)



Optical and microphysical characterization of aerosol layers

E. Giannakaki et al.

Groß, S., Esselborn, M., Weinzierl, B., Wirth, M., Fix, A., and Petzold, A.: Aerosol classification by airborne high spectral resolution lidar observations, *Atmos. Chem. Phys.*, 13, 2487–2505, doi:10.5194/acp-13-2487-2013, 2013.

Hänel, A., Baars, H., Althausen, D., Ansmann, A., Engelmann, R., and Sun, Y. J.: One-year aerosol profiling with EUCAARI Raman lidar at Shangdianzi GAW station: Beijing plume and seasonal variation, *J. Geophys. Res.*, 117, D13201, doi:10.1029/2012JD017577, 2012.

Heese, B., Althausen, D., Baars, H., Bohlmann, S., and Deng, R.: Aerosol properties over Southeastern China from multiwavelength Raman and depolarization lidar measurements, in: Reviewed and Revised Papers of 27th ILRC International Laser Radar Conference, 5–10 July 2015, New York, USA, 2015.

Ichoku, C., Remer, L. A., Kaufman, Y. J., Levy, R., Chu, D. A., Tanre, D., and Holben, B. N.: MODIS observation of aerosols and estimation of aerosol radiative forcing over southern Africa during SAFARI 2000, *J. Geophys. Res.*, 108, 8499, doi:10.1029/2002jd002366, 2003.

Illingworth, A. J., Barker, H. W., Beljaars, A., Ceccaldi, M., Chepfer, H., Cole, J., Delanoë, J., Domenech, C., Donovan, D. P., Fukuda, S., Hirakata, M., Hogan, R. J., Huenerbein, A., Kollias, P., Kubota, T., Nakajima, T., Nakajima, T. Y., Nishizawa, T., Ohno, Y., Okamoto, H., Oki, R., Sato, K., Satoh, M., Shephard, M., Wandinger, U., Wehr, T., and Van Zadelhoff, G.-J.: The Earthcare Satellite: the next step forward in global measurements of clouds, aerosols, precipitation and radiation, *B. Am. Meteorol. Soc.*, 96, 1311–1332, doi:10.1175/BAMS-D-12-00227.1, 2015.

IPCC: The Physical Science Basis, Contribution of Working Group I to the Fifth Assessment Report of the Intergovernmental Panel on Climate Change, edited by: Stocker, T. F., Qin, D., Plattner, G.-K., Tignor, M., Allen, S. K., Boschung, J., Nauels, A., Xia, Y., Bex, V., and Midgley, P. M., Cambridge University Press, Cambridge, UK, New York, NY, USA, 2013.

Kanitz, T., Ansmann, A., Engelmann, R., and Althausen, D.: North–south cross sections of the vertical aerosol distribution over the Atlantic Ocean from multiwavelength Raman/polarization lidar during Polarstern cruises, *J. Geophys. Res.*, 118, 2643–2655, doi:10.1002/jgrd.50273, 2013.

Kanitz, T., Engelmann, R., Heinold, B., Baars, H., Skupin, A., and Ansmann, A.: Tracking the Saharan Air Layer with shipborne lidar across the tropical Atlantic, *Geophys. Res. Lett.*, 41, 1044–1050, doi:10.1002/2013GL058780, 2014.

Klett, J. D.: Stable analytical inversion solution for processing lidar returns, *Appl. Optics*, 20, 211–220, doi:10.1364/AO.20.000211, 1981.

[Title Page](#)

[Abstract](#)

[Introduction](#)

[Conclusions](#)

[References](#)

[Tables](#)

[Figures](#)

◀

▶

◀
Back

▶
Close

[Full Screen / Esc](#)

[Printer-friendly Version](#)

[Interactive Discussion](#)



Komppula, M., Mielonen, T., Arola, A., Korhonen, K., Lihavainen, H., Hyvärinen, A.-P., Baars, H., Engelmann, R., Althausen, D., Ansmann, A., Müller, D., Panwar, T. S., Hooda, R. K., Sharma, V. P., Kerminen, V.-M., Lehtinen, K. E. J., and Viisanen, Y.: Technical Note: One year of Raman-lidar measurements in Gual Pahari EUCAARI site close to New Delhi in India – Seasonal characteristics of the aerosol vertical structure, *Atmos. Chem. Phys.*, 12, 4513–4524, doi:10.5194/acp-12-4513-2012, 2012.

Kulmala, M., Asmi, A., Lappalainen, H. K., Baltensperger, U., Brenguier, J.-L., Facchini, M. C., Hansson, H.-C., Hov, Ø., O'Dowd, C. D., Pöschl, U., Wiedensohler, A., Boers, R., Boucher, O., de Leeuw, G., Denier van der Gon, H. A. C., Feichter, J., Krejci, R., Laj, P., Lihavainen, H., Lohmann, U., McFiggans, G., Mentel, T., Pilinis, C., Riipinen, I., Schulz, M., Stohl, A., Swietlicki, E., Vignati, E., Alves, C., Amann, M., Ammann, M., Arabas, S., Artaxo, P., Baars, H., Beddows, D. C. S., Bergström, R., Beukes, J. P., Bilde, M., Burkhardt, J. F., Canonaco, F., Clegg, S. L., Coe, H., Crumeyrolle, S., D'Anna, B., Decesari, S., Gilardoni, S., Fischer, M., Fjaeraa, A. M., Fountoukis, C., George, C., Gomes, L., Halloran, P., Hamburger, T., Harrison, R. M., Herrmann, H., Hoffmann, T., Hoose, C., Hu, M., Hyvärinen, A., Hörrak, U., Inuma, Y., Iversen, T., Josipovic, M., Kanakidou, M., Kiendler-Scharr, A., Kirkevåg, A., Kiss, G., Klimont, Z., Kolmonen, P., Komppula, M., Kristjánsson, J.-E., Laakso, L., Laaksonen, A., Labonnote, L., Lanz, V. A., Lehtinen, K. E. J., Rizzo, L. V., Makkonen, R., Manninen, H. E., McMeeking, G., Merikanto, J., Minikin, A., Mirme, S., Morgan, W. T., Nemitz, E., O'Donnell, D., Panwar, T. S., Pawlowska, H., Petzold, A., Pienaar, J. J., Pio, C., Plass-Duelmer, C., Prévôt, A. S. H., Pryor, S., Reddington, C. L., Roberts, G., Rosenfeld, D., Schwarz, J., Selander, Ø., Sellegrí, K., Shen, X. J., Shiraiwa, M., Siebert, H., Sierau, B., Simpson, D., Sun, J. Y., Topping, D., Tunved, P., Vaattovaara, P., Vakkari, V., Veefkind, J. P., Visschedijk, A., Vuollekoski, H., Vuolo, R., Wehner, B., Wildt, J., Woodward, S., Worsnop, D. R., van Zadelhoff, G.-J., Zardini, A. A., Zhang, K., van Zyl, P. G., Kerminen, V.-M., Carslaw, K., and Pandis, S. N.: General overview: European Integrated project on Aerosol Cloud Climate and Air Quality interactions (EUCAARI) – integrating aerosol research from nano to global scales, *Atmos. Chem. Phys.*, 11, 13061–13143, doi:10.5194/acp-11-13061-2011, 2011.

Laakso, L., Vakkari, V., Virkkula, A., Laakso, H., Backman, J., Kulmala, M., Beukes, J. P., van Zyl, P. G., Tiitta, P., Josipovic, M., Pienaar, J. J., Chiloane, K., Gilardoni, S., Vignati, E., Wiedensohler, A., Tuch, T., Birmili, W., Piketh, S., Collett, K., Fourie, G. D., Komppula, M., Lihavainen, H., de Leeuw, G., and Kerminen, V.-M.: South African EUCAARI measurements:

Optical and microphysical characterization of aerosol layers

E. Giannakaki et al.

[Title Page](#)

[Abstract](#)

[Introduction](#)

[Conclusions](#)

[References](#)

[Tables](#)

[Figures](#)



[Back](#)

[Close](#)

[Full Screen / Esc](#)

[Printer-friendly Version](#)

[Interactive Discussion](#)



seasonal variation of trace gases and aerosol optical properties, *Atmos. Chem. Phys.*, 12, 1847–1864, doi:10.5194/acp-12-1847-2012, 2012.

5 Lourens, A. S. M., Butler, T. M., Beukes, J. P., van Zyl, P. G., Beirle, S., Wagner, T. K., Heue, K. P., Pienaar, J. J., Fourie, G. D., and Lawrence, M. G.: Re-evaluating the NO₂ hotspot over the South African Highveld, *S. Afr. J. Sci.*, 108, 54–59, doi:10.4102/sajs.v108i11/12.1146, 2012.

Mamouri, R. E. and Ansmann, A.: Fine and coarse dust separation with polarization lidar, *Atmos. Meas. Tech.*, 7, 3717–3735, doi:10.5194/amt-7-3717-2014, 2014.

10 Mamouri, R. E., Ansmann, A., Nisantzi, A., Kokkalis, P., Schwarz, A., and Hadjimitsis, D.: Low Arabian dust extinction-to-backscatter ratio, *Geophys. Res. Lett.*, 40, 4762–4766, doi:10.1002/grl.50898, 2013.

Mishchenko, M., Travis, L. D., Kahn, R. A., and West, R. A.: Modeling phase functions for dustlike tropospheric aerosols using a shape mixture of randomly oriented polydisperse spheroids, *J. Geophys. Res.*, 102, 16831–16847, 1997.

15 Müller, D., Wandinger, U., and Ansmann, A.: Microphysical particle parameters from extinction and backscatter lidar data by inversion with regularization: theory, *Appl. Optics*, 38, 2346–2357, 1999a.

Müller, D., Wandinger, U., and Ansmann, A.: Microphysical particle parameters from extinction and backscatter lidar data by inversion with regularization: simulation, *Appl. Optics*, 38, 2358–2368, 1999b.

20 Müller, D., Wandinger, U., Althausen, D., and Fiebig, M.: Comprehensive particle characterization from three-wavelength Raman-lidar observations, *Appl. Optics*, 40, 4863–4869, doi:10.1364/AO.40.004863, 2001.

25 Müller, D., Mattis, I., Wandinger, U., Ansmann, A., Althausen, D., Dubovik, O., Eckhardt, S., and Stohl, A.: Saharan dust over a central European EARLINET-AERONET site: combined observations with Raman lidar and Sun photometer, *J. Geophys. Res.*, 108, 4345, doi:10.1029/2002JD002918, 2003.

30 Müller, D., Mattis, I., Wandinger, U., Ansmann, A., Althausen, D., and Stohl, A.: Raman lidar observations of aged Siberian and Canadian forest fire smoke in the free troposphere over Germany in 2003: microphysical particle characterization, *J. Geophys. Res.*, 110, D17201, doi:10.1029/2004JD005756, 2005.

Title Page

Abstract

Introduction

Conclusions

References

Tables

Figures

◀

▶

◀

▶

Back

Close

Full Screen / Esc

Printer-friendly Version

Interactive Discussion



- Müller, D., Ansmann, A., Mattis, I., Tesche, M., Wandinger, U., Althausen, D., and Pissani, G.: Aerosol-type dependent lidar ratios observed with Raman lidar, *J. Geophys. Res.*, 12, D16202, doi:10.1029/2006JD008292, 2007.
- Murayama, T., Okamoto, H., Kaneyasu, N., Kamataki, H., and Miura, K.: Application of lidar depolarization measurement in the atmospheric boundary layer: effects of dust and sea-salt particles, *J. Geophys. Res.*, 104, 31781–31792, doi:10.1029/1999JD900503, 1999.
- Murayama, T., Masonis, S. J., Redemann, J., Aderson, T. L., Schmid, B., Living, J. M., Russell, P. B., Huebert, B., Howell, S. G., McNaughton, C. S., Clarke, A., Abo, M., Shimizu, A., Sugimoto, N., Yabuki, M., Kuze, H., Fukagawa, S., Maxwell-Meier, K., Weber, R. J., Orsini, D. A., Blomquist, B., Bandy, A., and Thornton, D.: An intercomparison of lidar-derived aerosol optical properties with airborne measurements near Toko during ACE-Asia, *J. Geophys. Res.*, 108, 8651, doi:10.1029/2002JD003259, 2003.
- Murayama, T., Müller, D., Wada, K., Shimizu, A., Sekigushi, M., and Tsukamoto, T.: Characterization of Asian dust and Siberian smoke with multi-wavelength Raman lidar over Tokyo, Japan in spring 2003, *Geophys. Res. Lett.*, 31, L23103, doi:10.1029/2004GL021105, 2004.
- Nicolae, D., Nemuc, A., Müller, D., Talianu, C., Vasilescu, J., Belegante, L., and Kolgotin, A.: Characterization of fresh and aged biomass burning events using multiwavelength Raman lidar and mass spectrometry, *J. Geophys. Res.*, 118, 2956–2965, doi:10.1002/jgrd.50324, 2013.
- Nisantzi, A., Mamouri, R. E., Ansmann, A., and Hadjimitsis, D.: Injection of mineral dust into the free troposphere during fire events observed with polarization lidar at Limassol, Cyprus, *Atmos. Chem. Phys.*, 14, 12155–12165, doi:10.5194/acp-14-12155-2014, 2014.
- Noh, Y. M., Müller, D., Shin, D. H., Lee, H. L., Jung, J. S., Lee, K. H., Cribb, M., Li, Z., and Kim, Y. J.: Optical and microphysical properties of severe haze and smoke aerosol measured by integrated remote sensing techniques in Gwangju, Korea, *Atmos. Environ.*, 43, 879–888, doi:10.1016/j.atmosenv.2008.10.058, 2009.
- Omar, A., Winker, D., Vaughan, M., Hu, Y., Trepte, C., Ferrare, R., Lee, K., Hostetler, C., Kittaka, C., Rogers, R., Kuehn, R., and Liu, Z.: The CALIPSO automated aerosol classification and lidar ratio selection algorithm, *J. Atmos. Ocean. Tech.*, 26, 1994–2014, doi:10.1175/2009JTECHA1231.1, 2009.
- Piketh, S. J., Tyson, P. D., and Steffen, W.: Aeolian transport from southern Africa and iron fertilization of marine biota in the South Indian Ocean, *S. Afr. J. Sci.*, 96, 244–246, 2000.

[Title Page](#)[Abstract](#)[Introduction](#)[Conclusions](#)[References](#)[Tables](#)[Figures](#)[◀](#)[▶](#)[◀](#)[▶](#)[Back](#)[Close](#)[Full Screen / Esc](#)[Printer-friendly Version](#)[Interactive Discussion](#)

- Piketh, S. J., Swap, R. J., Maenhaut, W., Annegarn, H. J., and Formenti, P.: Chemical evidence of long-range atmospheric transport over southern Africa, *J. Geophys. Res.*, 107, 4817, doi:10.1029/2002jd002056, 2002.
- Pósfai, M., Simonics, R., Li, J., Hobbs, P. V., and Buseck, P. R.: Individual aerosol particles from biomass burning in southern Africa: 1. Compositions and size distributions of carbonaceous particles, *J. Geophys. Res.*, 108, 2156–2202, doi:10.1029/2002JD002291, 2003.
- Preißler, J., Bravo-Aranda, J., Wagner, F., Granados-Muñoz, M. J., Navas-Guzmán, F., Guerrero-Rascado, J. L., Lyamani, H., and Alados-Arboledas, L.: Optical properties of free tropospheric aerosol from multi-wavelength Raman lidars over the southern Iberian Peninsula, in: Proceedings of the 9th International Symposium on Tropospheric Profiling, l'Aquila, Italy, 3–7 September 2012, ISBN 978-90-815839-4-7, 2012.
- Preißler, J., Wagner, F., Guerrero-Rascado, J. L., and Silva, A. M.: Two years of free-tropospheric aerosol layers observed over Portugal by lidar, *J. Geophys. Res.*, 118, 3676–3686, doi:10.1002/jgrd.50350, 2013.
- Queface, A. J., Piketh, S. J., Eck, T. F., Tsay, S. C., and Mavume, A. F.: Climatology of aerosol optical properties in Southern Africa, *Atmos. Environ.*, 45, 2910–2921, doi:10.1016/j.atmosenv.2011.01.056, 2011.
- Radke, L. F., Heggs, D. A., Lyons, H., Brook, C. A., Hobbs, P. V., Weiss, R., and Rasmussen, R.: Airborne measurements on smoke from biomass burning, in: *Aerosols and Climate*, edited by: Hobbs, P. V. and McCormick, M. P., Deepak, A., Hampton, VA, USA, 411–422, 1998.
- Reid, J. S. and Hobbs, P. V.: Physical and optical properties of smoke from individual biomass fires in Brazil, *J. Geophys. Res.*, 103, 32013–32031, doi:10.1029/98JD00159, 1998.
- Reid, J. S., Koppmann, R., Eck, T. F., and Eleuterio, D. P.: A review of biomass burning emissions part II: intensive physical properties of biomass burning particles, *Atmos. Chem. Phys.*, 5, 799–825, doi:10.5194/acp-5-799-2005, 2005.
- Ross, K. E., Piketh, S. J., Bruintjes, R. T., Burger, R. P., Swap, R. J., and Annegarn, H. J.: Spatial and seasonal variations in CCN distribution and the aerosol-CCN relationship over southern Africa, *J. Geophys. Res.*, 108, 8481, doi:10.1029/2002JD002384, 2003.
- Roy, D. P., Frost, P. G. H., Justice, C. O., Landmann, T., Le Roux, J. L., Gumbo, K., Makungwa, S., Dunham, K., du Toit, R., Mhwandagara, K., Zacarias, A., Tacheba, B., Dube, O. P., Pereira, J. M. C., Mushove, P., Morisette, J. T., Santhana-Vannan, S. K., and Davies, D.: The Southern Africa Fire Network (SAFnet) regional burned-area product-validation protocol, *Int. J. Remote Sens.*, 26, 4265–4292, 2005.

Optical and microphysical characterization of aerosol layers

E. Giannakaki et al.

[Title Page](#)

[Abstract](#)

[Introduction](#)

[Conclusions](#)

[References](#)

[Tables](#)

[Figures](#)

◀

▶

◀

▶

[Back](#)

[Close](#)

[Full Screen / Esc](#)

[Printer-friendly Version](#)

[Interactive Discussion](#)



- Roy, D. P., Boschetti, L., Justice, C. O., and Ju, J.: The collection 5 MODIS burned area product – global evaluation by comparison with the MODIS active fire product, *Remote Sens. Environ.*, 112, 3960–3707, doi:10.1016/j.rse.2008.05.013, 2008.
- Schneider, P., Lahoz, W. A., and van der A, R.: Recent satellite-based trends of tropospheric nitrogen dioxide over large urban agglomerations worldwide, *Atmos. Chem. Phys.*, 15, 1205–1220, doi:10.5194/acp-15-1205-2015, 2015.
- Shimizu, A., Sugimoto, N., Matsui, I., Arao, K., Uno, I., Murayama, T., Kagawa, N., Aoki, K., Uchiyama, A., and Yamazaki, A.: Continuous observations of Asian dust and other aerosols by polarization lidars in China and Japan during ACE-Asia, *J. Geophys. Res.*, 109, D19S17, doi:10.1029/2002JD003253, 2004.
- Shin, S.-K., Müller, D., Lee, C., Lee, K. H., Shin, D., Kim, Y. J., and Noh, Y. M.: Vertical variation of optical properties of mixed Asian dust/pollution plumes according to pathway of air mass transport over East Asia, *Atmos. Chem. Phys.*, 15, 6707–6720, doi:10.5194/acp-15-6707-2015, 2015.
- Sugimoto, N., Uno, I., Nishikawa, M., Shimizu, A., Matsui, I., Dong, X., Chen, Y., and Quan, H.: Record heavy Asian dust in Beijing in 2002: observations and model analysis of recent events, *Geophys. Res. Lett.*, 30, 1640, doi:10.1029/2002GL016349, 2003.
- Tesche, M., Ansmann, A., Müller, D., Althausen, D., Engelmann, R., Freudenthaler, V., and Groß, S.: Vertically resolved separation of dust and smoke over Cape Verde using multiwavelength Raman and polarization lidars during Saharan Mineral Dust Experiment 2008, *J. Geophys. Res.*, 114, D13202, doi:10.1029/2009JD011862, 2009.
- Tesche, M., Gross, S., Ansmann, A., Müller, D., Althausen, D., Freudenthaler, V., and Esselborn, M.: Profiling of Saharan dust and biomass-burning smoke with multiwavelength polarization Raman lidar at Cape Verde, *Tellus B*, 63, available at: <http://www.tellusb.net/index.php/tellusb/article/view/16360> (last access: 14 December 2015), 2011.
- Tesfaye, M., Sivakumar, V., Botai, J., and Tsidu, G. M.: Aerosol climatology over South Africa based on 10 years of Multiangle Imaging Spectroradiometer (MISR) data, *J. Geophys. Res.*, 116, D20216, doi:10.1029/2011jd016023, 2011.
- Tiitta, P., Vakkari, V., Croteau, P., Beukes, J. P., van Zyl, P. G., Josipovic, M., Venter, A. D., Jaars, K., Pienaar, J. J., Ng, N. L., Canagaratna, M. R., Jayne, J. T., Kerminen, V.-M., Kokkola, H., Kulmala, M., Laaksonen, A., Worsnop, D. R., and Laakso, L.: Chemical composition, main sources and temporal variability of PM₁ aerosols in southern African grassland, *Atmos. Chem. Phys.*, 14, 1909–1927, doi:10.5194/acp-14-1909-2014, 2014.

Optical and microphysical characterization of aerosol layers

E. Giannakaki et al.

[Title Page](#)

[Abstract](#)

[Introduction](#)

[Conclusions](#)

[References](#)

[Tables](#)

[Figures](#)

◀

▶

◀

▶

[Back](#)

[Close](#)

[Full Screen / Esc](#)

[Printer-friendly Version](#)

[Interactive Discussion](#)



Twomey, S.: Introduction to the Mathematics of Inversion in Remotes Sensing and Indirect Measurements, Elsevier Scientific, New York, USA, 1977.

Venter, A. D., Vakkari, V., Beukes, J. P., van Zyl, P. G., Laakso, H., Mabaso, D., Tiitta, P., Josipovic, M., Kulmala, M., Pienaar, J. J., and Laakso, L.: An air quality assessment in the industrialised western Bushveld Igneous Complex, South Africa, *S. Afr. J. Sci.*, 108, 1059, doi:10.4102/sajs.v108i9/10.1059, 2012.

Veselovskii, I., Kolgotin, A., Griaznov, V., Müller, D., Wandinger, U., and Whiteman, D. N.: Inversion with regularization for the retrieval of tropospheric aerosol parameters from multiwavelength lidar sounding, *Appl. Optics*, 41, 3685–3699, 2002.

Veselovskii, I., Kolgotin, A., Griaznov, V., Müller, D., Franke, K., and Whiteman, D. N.: Inversion of multiwavelength Raman lidar data for retrieval of bimodal aerosol size distribution, *Appl. Optics*, 43, 1180–1195, 2004.

Wandinger, U. and Ansmann, A.: Experimental determination of the lidar overlap profile with Raman lidar, *Appl. Optics*, 41, 511–514, doi:10.1364/AO.41.000511, 2002.

Wandinger, U., Müller, D., Böckmann, C., Althausen, D., Matthias, V., Bösenberg, J., Weiβ, V., Fiebig, M., Wendisch, M., Stohl, A., Ansmann, A.: Optical and microphysical characterization of biomass burning and industrial-pollution aerosols from multiwavelength lidar and aircraft measurements, *J. Geophys. Res.*, 107, 8125, doi:10.1029/2000JD000202, 2002.

Weinzierl, B., Sauer, D., Esselborn, M., Petzold, A., Veira, A., Rose, M., Mund, S., Wirth, M., Ansmann, A., Tesche, M., Gross, S., and Freudenthaler, V.: Microphysical and optical properties of dust and tropical biomass burning aerosol layers in the Cape Verde region – an overview of the airborne in situ and lidar measurements during SAMUM-2, *Tellus B*, 63, 589–618, doi:10.1111/j.1600-0889.2011.00566.x, 2011.

Wenig, M., Spichtinger, N., Stohl, A., Held, G., Beirle, S., Wagner, T., Jähne, B., and Platt, U.: Intercontinental transport of nitrogen oxide pollution plumes, *Atmos. Chem. Phys.*, 3, 387–393, doi:10.5194/acp-3-387-2003, 2003.

Winkler, H., Formenti, P., Esterhuyse, D. J., Swap, R. J., Helas, G., Anne garn, H. J., and Andreae, M. O.: Evidence for large-scale transport of biomass burning aerosols from sunphotometry at a remote South African site: *Atmos. Environ.*, 42, 5569–5578, doi:10.1016/j.atmosenv.2008.03.031, 2008.

Title Page

Abstract

Introduction

Conclusions

References

Tables

Figures



◀
Back

▶
Close

Full Screen / Esc

Printer-friendly Version

Interactive Discussion



Table 1. Aerosol type, time and altitude range of aerosol layers used for optical and microphysical aerosol characterization.

aerosol source	date	time [UTC]	height [m]
urban/industrial	25 Mar 2010	18:00–19:50	2100–2670
	25 Mar 2010	18:00–19:50	2790–3450
	25 Mar 2010	18:00–19:50	1980–2250
	16 Apr 2010	21:20–23:54	2280–2520
	16 Apr 2010	21:20–23:54	2280–2520
	16 Apr 2010	21:20–23:54	2610–3170
	14 May 2010	18:00–00:00	930–1360
	15 May 2010	18:30–20:20	1380–1860
	15 May 2010	18:30–20:20	2250–2700
	30 Nov 2010	17:15–18:00	960–1300
	30 Nov 2010	17:15–18:00	1350–1920
	30 Jun 2010	17:00–18:00	1420–1620
	30 Jun 2010	17:00–18:00	1650–1830
	10 Jan 2011	19:15–20:15	1890–2160
	13 Jan 2011	21:00–22:00	1200–1800
	13 Jan 2011	21:00–22:00	1920–2250
	13 Jan 2011	21:00–22:00	2430–2880
biomass burning	1 Oct 2010	00:10–01:00	1090–1900
	5 Oct 2010	18:10–23:10	1115–1750
	5 Oct 2010	18:10–23:10	1980–2700
	6 Oct 2010	20:00–00:00	1175–1540
	6 Oct 2010	20:00–00:00	1565–2160
	6 Oct 2010	20:00–00:00	2190–2520
	6 Oct 2010	20:00–00:00	2610–2820
	21 Oct 2010	01:30–02:30	880–1530
	21 Oct 2010	01:30–02:30	1685–2280
	21 Oct 2010	01:30–02:30	2400–2880
	22 Aug 2010	00:00–01:00	1205–1565
	22 Aug 2010	00:00–01:00	1685–1920
	22 Aug 2010	02:00–03:00	1115–1535
	22 Aug 2010	02:00–03:00	1745–2250
mixture of biomass burning desert dust	16 Aug 2010	17:00–18:00	1115–1445
	16 Aug 2010	19:00–20:00	995–1265
	18 Aug 2010	19:00–20:00	1175–1355
	18 Aug 2010	19:00–20:00	1415–1715
	18 Aug 2010	19:00–20:00	1865–2160
	22 Aug 2010	17:00–18:00	1145–1505
	22 Aug 2010	17:00–18:00	1595–2040

Optical and microphysical characterization of aerosol layers

E. Giannakaki et al.

Title Page

Abstract

Introduction

Conclusions

References

Tables

Figures



Back

Close

Full Screen / Esc

Printer-friendly Version

Interactive Discussion



Table 2. Mean value \pm standard deviation of aerosol lidar ratio at 355, particle depolarization ratio and Ångström exponent related to extinction between 355 and 532 nm for the examined aerosol types, as well as value of range and median.

aerosol source	mean \pm SD	range	median
lidar ratio at 355 nm [sr]			
urban/industrial	52 \pm 7	41–59	54
biomass burning	92 \pm 10	81–119	88
biomass burning and desert dust	74 \pm 11	59–90	90
lidar ratio at 532 nm [sr]			
urban/industrial	41 \pm 13	23–74	38
biomass burning	75 \pm 14	47–92	79
biomass burning & desert dust	46 \pm 13	33–68	40
particle depolarization ratio at 355 nm [%]			
urban/industrial	0.9 \pm 0.4	0.3–1.7	1.0
biomass burning	3.2 \pm 1.3	1.2–5.7	2.7
biomass burning and desert dust	8.3 \pm 0.7	7.3–9.1	8.1
Ångström exponent related to extinction between 355 and 532 nm			
urban/industrial	2.3 \pm 0.5	1.3–3.0	2.4
biomass burning	1.7 \pm 0.3	1.0–2.4	1.7
biomass burning and desert dust	2.0 \pm 0.4	1.6–2.5	2.0

Optical and microphysical characterization of aerosol layers

E. Giannakaki et al.

[Title Page](#)

[Abstract](#)

[Introduction](#)

[Conclusions](#)

[References](#)

[Tables](#)

[Figures](#)

◀

▶

◀

▶

[Back](#)

[Close](#)

[Full Screen / Esc](#)

[Printer-friendly Version](#)

[Interactive Discussion](#)



Table 3. Mean value \pm standard deviation of effective radius and single-scattering albedo for the examined aerosol types, as well as range and median.

Aerosol Source	mean \pm SD	range	median
effective radius [μm]			
urban/industrial	0.10 ± 0.03	0.07–0.16	0.09
biomass burning	0.17 ± 0.04	0.11–0.28	0.17
biomass burning and desert dust	0.13 ± 0.03	0.09–0.19	0.13
single-scattering albedo at 532 nm			
urban/industrial	0.87 ± 0.06	0.75–0.96	0.88
biomass burning	0.90 ± 0.06	0.77–0.98	0.90
biomass burning and desert dust	0.88 ± 0.07	0.76–0.95	0.89
complex refractive index			
urban/industrial	$1.61 (\pm 0.11) + 0.021 (\pm 0.010)i$	1.47–1.78 (RRI) 0.007–0.039 (IRI)	1.64 (RRI) 0.020 (IRI)
biomass burning	$1.43 (\pm 0.07) + 0.016 (\pm 0.011)i$	1.35–1.57 (RRI) 0.002–0.046 (RRI)	1.40 (RRI) 0.015 (IRI)
biomass burning and desert dust	$1.52 (\pm 0.15) + 0.022 (\pm 0.015)i$	1.33–1.74 (RRI) 0.004–0.046 (IRI)	1.56 (RRI) 0.019 (IRI)

Title Page

Abstract

Introduction

Conclusions

References

Tables

Figures

◀

▶

◀

▶

Back

Close

Full Screen / Esc

Printer-friendly Version

Interactive Discussion



**Optical and
microphysical
characterization of
aerosol layers**

E. Giannakaki et al.

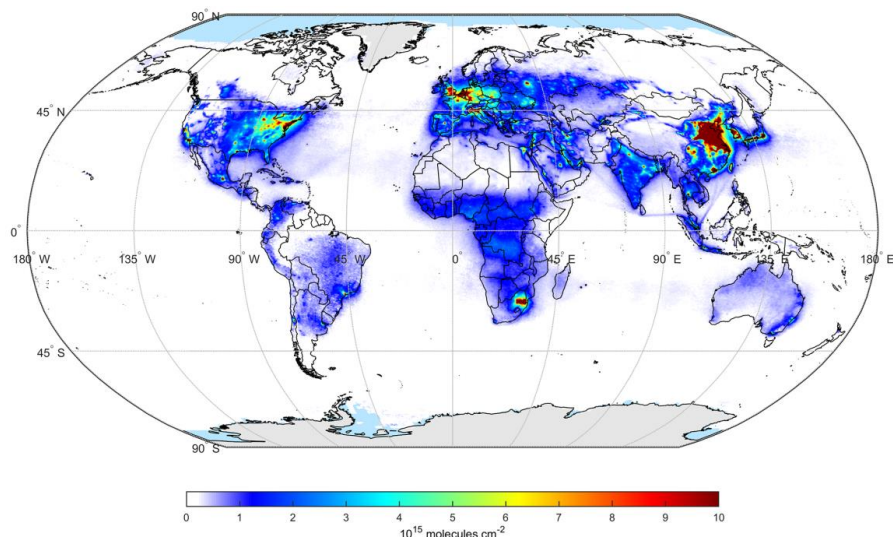


Figure 1. Global map of long-term average tropospheric NO_2 column derived from SCIAMACHY data from August 2002 to March 2012 (Schneider et al., 2015).

[Title Page](#)[Abstract](#)[Introduction](#)[Conclusions](#)[References](#)[Tables](#)[Figures](#)[Back](#)[Close](#)[Full Screen / Esc](#)[Printer-friendly Version](#)[Interactive Discussion](#)

Optical and microphysical characterization of aerosol layers

E. Giannakaki et al.

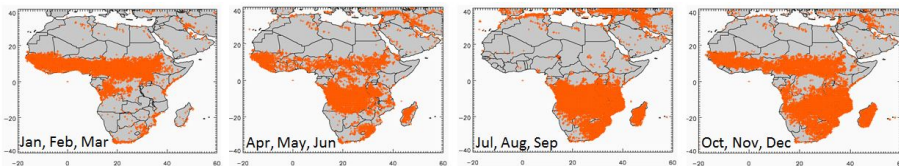


Figure 2. Number of hotspots with confidence levels between 80–100 % averaged in terms of 3 months for the year 2010 in the latitude range between –40 and 40° and longitude range between –20 and 60° .

[Title Page](#)[Abstract](#)[Introduction](#)[Conclusions](#)[References](#)[Tables](#)[Figures](#)[◀](#)[▶](#)[Back](#)[Close](#)[Full Screen / Esc](#)[Printer-friendly Version](#)[Interactive Discussion](#)

Optical and microphysical characterization of aerosol layers

E. Giannakaki et al.

Title Page

Abstract

Introduction

Conclusions

References

Tables

Figures

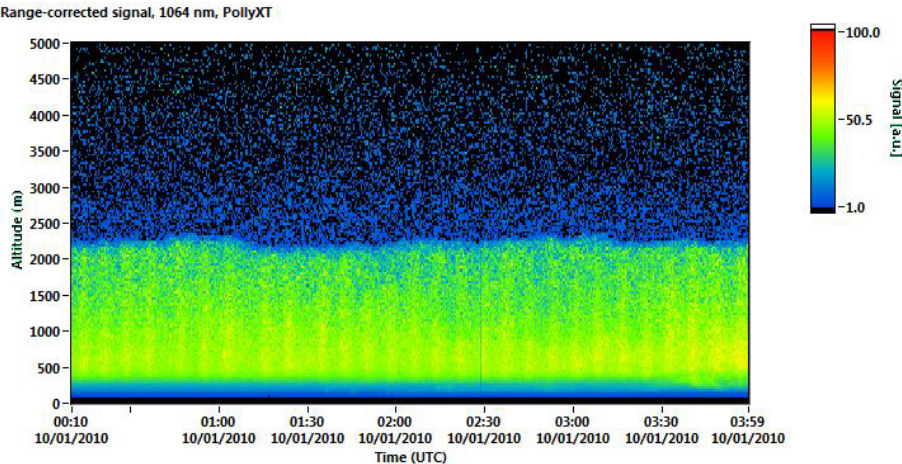


Figure 3. Temporal development of the range corrected signal at 1064 nm at Elandsfontein on 1 October 2010, 00:10–03:59 UTC. The resolution is 15 m in height and 30 s in time.

Optical and microphysical characterization of aerosol layers

E. Giannakaki et al.

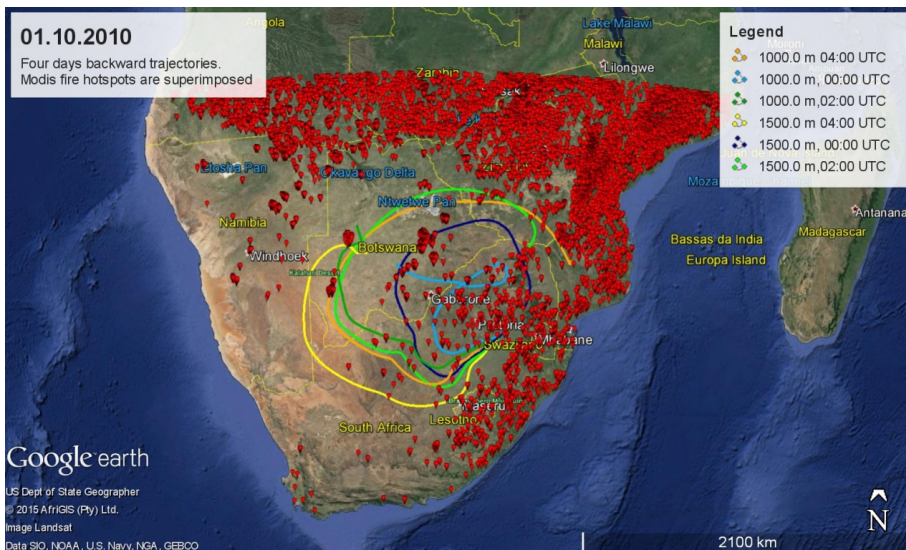


Figure 4. Four-day backward trajectories arriving at Elandsfontein on 1 October 2010 at 00:00, 02:00 and 04:00 UTC. The arrival heights above Elandsfontein are 10:00 and 15:00 UTC. MODIS fire hotspots are superimposed for the period 28 September–1 October 2010 and for the latitude range between -35 and -15° W and the longitude range between 10 and 40° S.

Title Page	Abstract	Introduction
Conclusions	References	
Tables	Figures	
		
Back	Close	
Full Screen / Esc		
Printer-friendly Version		
Interactive Discussion		

Optical and microphysical characterization of aerosol layers

E. Giannakaki et al.

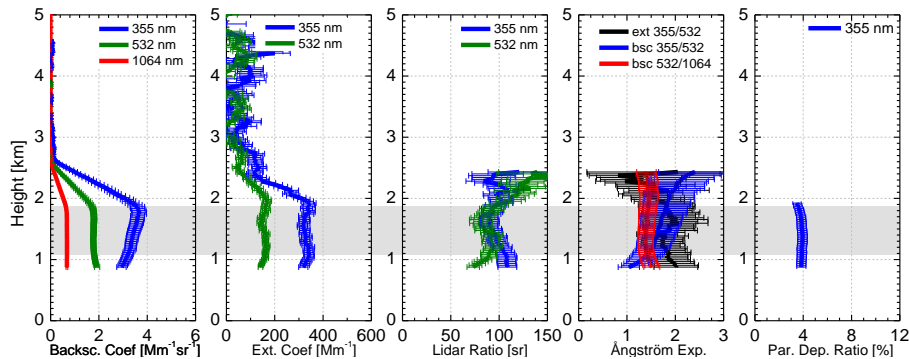


Figure 5. Backscatter coefficients, extinction coefficients, lidar ratios, Ångstrom exponents and particle depolarization ratio at Elandsfontein on 1 October 2010, 00:10–03:59 UTC.

Optical and microphysical characterization of aerosol layers

E. Giannakaki et al.

[Title Page](#)

[Abstract](#)

[Introduction](#)

[Conclusions](#)

[References](#)

[Tables](#)

[Figures](#)

[◀](#)

[▶](#)

[◀](#)

[▶](#)

[Back](#)

[Close](#)

[Full Screen / Esc](#)

[Printer-friendly Version](#)

[Interactive Discussion](#)

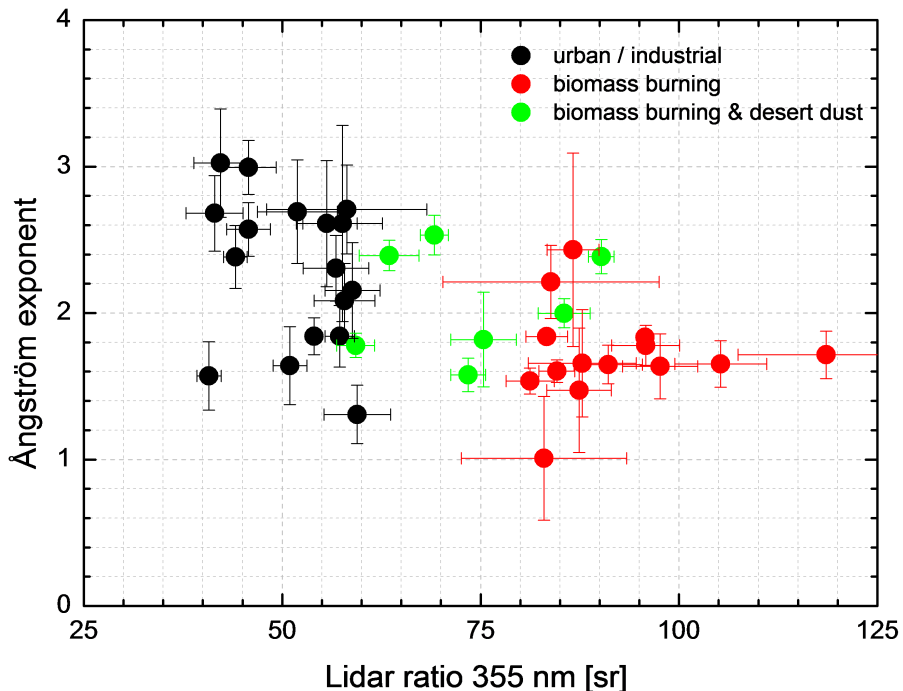


Figure 6. Lidar ratio at 355 nm vs. the extinction-related Ångström exponent from 355 to 532 nm for the three aerosol types investigated in our study.

Optical and microphysical characterization of aerosol layers

E. Giannakaki et al.

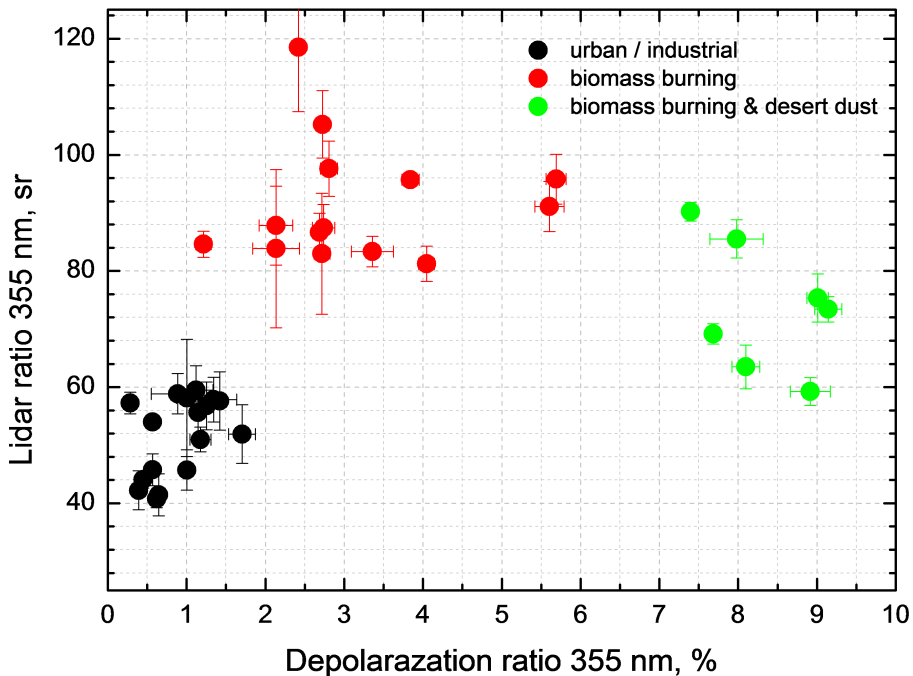


Figure 7. Lidar ratio at 355 nm vs. the depolarization ratio at 355 nm for the three aerosol types investigated in our study.



Optical and microphysical characterization of aerosol layers

E. Giannakaki et al.

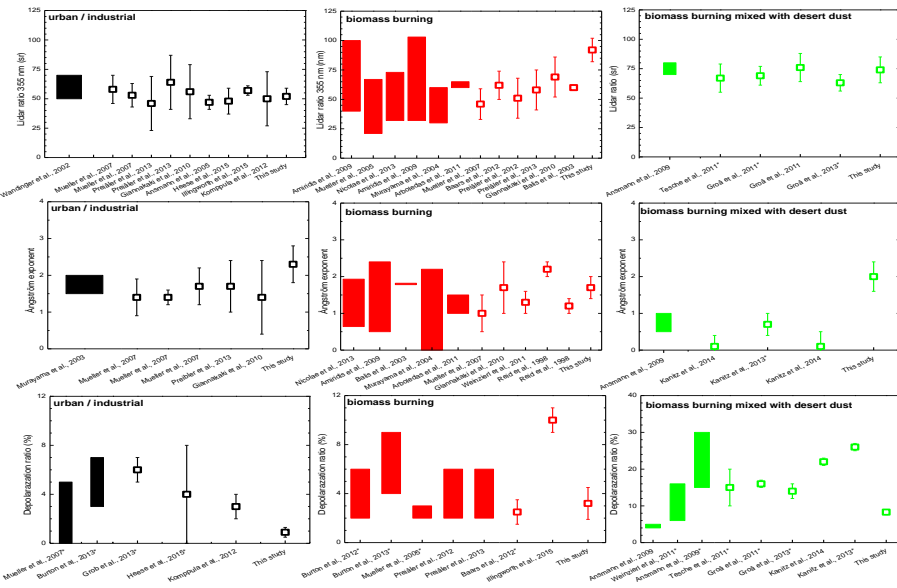


Figure 8. General literature values for lidar ratio at 355 nm, Ångström exponent and depolarization ratio (355 or 532 nm) for urban/industrial (black), biomass burning (red) and for mixed biomass burning with desert dust aerosols (green). Floating columns are referring to range values while the symbols are referring to mean values with one standard deviation.

Title Page	Abstract	Introduction
Conclusions	References	
Tables	Figures	
Back	Close	Full Screen / Esc
Printer-friendly Version		
Interactive Discussion		



Optical and microphysical characterization of aerosol layers

E. Giannakaki et al.

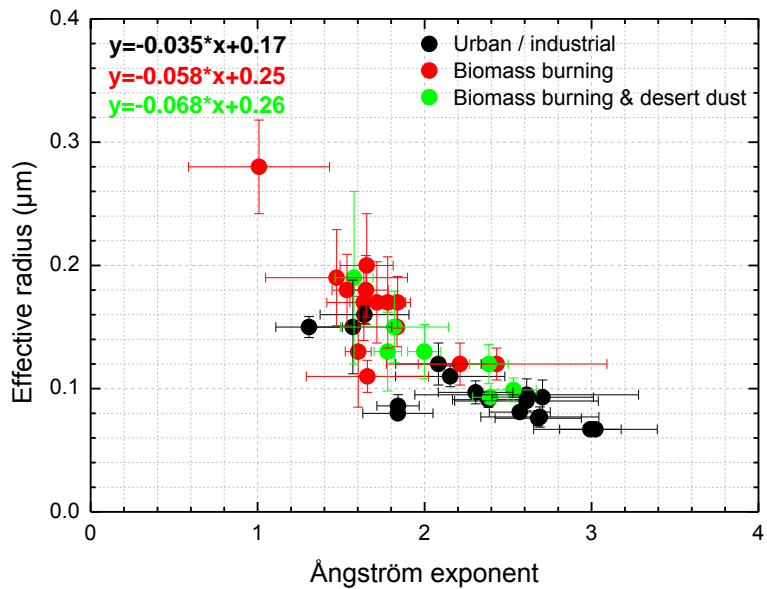


Figure 9. Effective radius vs. Ångström exponent for the three aerosol types investigated in our study.